Iran J Pharm Res. 2022 December; 21(1):e127035. doi: 10.5812/ijpr-127035.

Published online 2022 May 12. **Research Article**

Montmorillonite-Famotidine/Chitosan Bio-nanocomposite Hydrogels as a Mucoadhesive/Gastroretentive Drug Delivery System

Hassan Farhadnejad [1, 2], Seyed Alireza Mortazavi [1, *], Sanaz Jamshidfar [3], Amir Rakhshani [4], Hamidreza Motasadizadeh [4], Yousef Fatahi [4, 5, 6], Athar Mahdieh [4] and Behzad Darbasizadeh [1]

[1] Department of Pharmaceutics and Pharmaceutical Nanotechnology, School of Pharmacy, Shahid Beheshti University of Medical Sciences, Tehran, Iran
[2] Research and Development Department, Varian Pharmed Pharmaceutical Company, Tehran, Iran
[3] Department of Pharmaceutics, Faculty of Pharmacy, Tehran University of Medical Sciences, Tehran, Iran
[4] Department of Pharmaceutical Nanotechnology, Faculty of Pharmacy, Tehran University of Medical Sciences, Tehran, Iran
[5] Nanotechnology Research Center, Faculty of Pharmacy, Tehran University of Medical Sciences, Tehran, Iran
[6] Universal Scientific Education and Research Network, Tehran, Iran

[*] *Corresponding author*: Department of Pharmaceutics and Pharmaceutical Nanotechnology, School of Pharmacy, Shahid Beheshti University of Medical Sciences, Tehran, Iran. Email: mortazavisar@yahoo.com

Received 2021 August 22; **Revised** 2022 February 18; **Accepted** 2022 March 09.

Abstract

The main purpose of the present study was to fabricate mucoadhesive bio-nanocomposite hydrogels to prolong the drug retention time in the stomach. In these bio-nanocomposite hydrogels, chitosan (CH) was used as a bioadhesive matrix, montmorillonite (MMT) was applied to modulate the release rate, and tripolyphosphate (TPP) was the cross-linking agent. The test samples were analyzed via different methods such as X-ray diffraction (XRD), Fourier-transform infrared spectroscopy (FTIR), thermogravimetric analysis (TGA), and scanning electron microscopy (SEM). Drug incorporation efficacy and mucoadhesive strength of these nanocomposite hydrogel beads were studied. Swelling and in vitro drug release behaviors of these bio-nanocomposite hydrogels were evaluated in simulated gastric fluid (SGF; pH 1.2). The optimized MMT-famotidine (FMT)/CH bio-nanocomposite hydrogels displayed a controllable and sustainable drug release profile with suitable mucoadhesion and prolonged retention time in the stomach. Thus, the results demonstrated that the fabricated mucoadhesive bio-nanocomposite hydrogels could remarkably increase the therapeutic efficacy and bioavailability of FMT by the oral route.

Keywords: Bio-nanocomposite Hydrogel, Drug Delivery, Mucoadhesion, Gastroretention

1. Background

The oral route is the most usual and comfortable route for drug prescribing due to its higher patient compliance, low cost, painlessness, and flexibility in the formulation (1-4). However, the heterogeneity of the gastrointestinal (GI) system and the change in different factors, such as pH, enzymes, gastric retention time, and surface area, throughout the GI system significantly affect drug absorption (3, 5). Conventional and controlled drug delivery systems do not solely resolve these problems. Especially, these drug delivery systems are not suitable carriers for drugs with a narrow absorption window in the upper part of the GI system or drugs locally applied in the treatment of gastric diseases (6-8). In recent years, gastroretentive drug carriers have been evaluated for oral delivery of different drugs to resolve these difficulties (2, 9, 10). These formulations can sustain the drug release and increase the residence time of the drug in the upper part of the GI system, leading to complete absorption of the drug in the target site. Gastroretentive drug delivery systems enhance drug bioavailability, therapeutic effectiveness, and drug solubility for low soluble drugs and decrease drug waste. Thus, different types of pharmaceutical formulations, including floating, swellable, high-density, and mucoadhesive formulations, have been introduced as gastroretentive drug delivery systems (2, 11-14).

Among these formulations, mucoadhesive formulations have attracted much attention as gastroretentive drug delivery systems (15-17). These formulations can adhere to the epithelial surface, provide a proper interaction between the drug and target site, and enhance the retention time of the drug in the target site, resulting in its controlled release in a prolonged time period and decreasing the content of the drug needed to treat the disease (18). Hydrogels can act as mucoadhesive compounds. Different types of polymers, such as poly-lactic acid (PLA), carbopol, poly(acrylic acid), hydroxypropyl methylcellu-

Copyright © 2022, Author(s). This is an open-access article distributed under the terms of the Creative Commons Attribution-NonCommercial 4.0 International License (http://creativecommons.org/licenses/by-nc/4.0/) which permits copy and redistribute the material just in noncommercial usages, provided the original work is properly cited.

lose (HPMC), chitosan (CH), polyethylene glycol (PEG), and sodium alginate (SA) can be applied to fabricate mucoadhesive hydrogels (19-21). Hydrogel compounds, especially smart hydrogels, are extensively applied in the medical fields, such as drug delivery and tissue engineering (22-25). In recent years, smart nanocomposite hydrogels have attracted much attention as controlled drug delivery systems due to having improved properties compared to traditional hydrogels (26-29).

CH, a bioadhesive polysaccharide, is produced by the deacetylation of chitin in the presence of an alkaline substance such as sodium hydroxide (30). This polymer has been extensively studied as a drug delivery system due to its unique properties such as high bioadhesivity, proper viscosity, good molding ability, non-toxicity, low cost, excellent biocompatibility, bioactivity, and biodegradability (31-36). Due to the presence of many amine groups on its polymeric chains, CH can form spherical hydrogel compounds via cross-linking with multivalent anions such as tripolyphosphate (TPP) ions (31). However, some drugs, especially water-soluble drugs, are slightly loaded into hydrogel compounds based on polysaccharides. It can be a critical challenge in the fabrication of appropriate drug delivery systems. This phenomenon might arise from the sudden transfer of water-soluble drugs from these hydrogel compounds to the cross-linking medium. In addition, hydrogel compounds based on polysaccharide polymers possess slight stability in an aqueous medium and quickly degraded in the GI media, resulting in the initial burst release of drug from them (37, 38).

Different methods have been investigated to solve these problems; in this regard, adding mineral nanoparticles to these compounds can be an efficient method. The embedment of the mineral nanoparticles into the hydrogel matrix results in an increase in its hydrolytic strength, thereby leading to the release of drugs from it in a controllable and appropriate manner (38-40). For example, Hossieni-Aghdam et al. developed a method to enhance drug incorporation efficacy by coating atenolol–incorporated halloysite (HNT-AT) with a carboxymethyl cellulose (CMC) polymer. They found that HNT-AT/CMC compounds displayed an extended-release behavior, vouching that the HNT mineral particles loaded into the hydrogel matrix could prolong the release of the drug from it (38). Yadollahi et al. fabricated pH-sensitive CH-ZnO/IBU compounds to prolong the release of ibuprofen. Their results indicated that the ZnO nanoparticles improved the swelling degree and ibuprofen release behavior of these compounds (31).

Montmorillonite (MMT), a phyllo-silicate nano-clay, is composed of negatively charged and stacked layers. Each layer of MMT possesses an O–M–O (M = Mg, Al) octahedral sheet sandwiched between a pair of O–M–O (M = Si) tetrahedral sheets. The layers of this nano-clay are separated via the interlayer nano-space (41). MMT has many advantages, including high cation exchange capacity, high adsorption ability, low price, large specific surface area, and excellent bioavailability, biodegradability, and biocompatibility (8, 42, 43). MMT is widely applied to fabricate nanocomposite hydrogels as drug delivery systems (44-46). Till now, various drugs have been reported to incorporate into the interlayer space of MMT, such as 5-fluorouracil (47), propranolol (8), timolol maleate (48), and irinotecan (49). In addition, the negatively charged zones of MMT can have a strong electrostatic interaction with cationic polymeric chains, such as CH, and form unique nanocomposite hydrogels. These nanocomposite hydrogels possess excellent mucoadhesive properties, high hydrolytic strength, interlayer nano-space, and, therefore, excellent capacity to load different drugs into the interlayer space.

Famotidine (FMT) is a histamine-2 (H2) receptor antagonist administered orally to decrease stomach acid production and treat peptic ulcers and gastroesophageal reflux (50). FMT is a white-to-pale yellow crystal that is slightly dissolved in water. Also, it has a short biological half-life (2.5 - 3.5 h) and must be dosed four times a day to maintain the therapeutic range. Moreover, absorption of the FMT changes from the upper GI tract to the colon in the GI system due to high susceptibility to gastric degradation, leading to low absorption and poor bioavailability (51, 52). According to the problems mentioned above, designing mucoadhesive/gastroretentive delivery systems can be useful and suitable for such therapeutic agents.

2. Objectives

In this work, we designed a gastroretentive carrier based on mucoadhesive CH hydrogel and MMT particles for FMT extended delivery. For this purpose, we first synthesized MMT-FMT particles via the incorporation of FMT into the nano-space between layers of MMT. Then, we coated MMT-FMT particles with a CH mucoadhesive polymer via cross-linking CH macromolecules with TPP anions. Moreover, we carried out an in vitro drug release test to prove the efficacy of MMT-FMT/CH bio-nanocomposite samples as gastroretentive/mucoadhesive drug delivery systems.

3. Methods

3.1. Materials

CH, 76% deacetylated, low MW and viscosity 122 cP, 1 wt% in H2O and sodium-MMT (MMT-Na, $(Na, Ca)_{0.33}(Al, Mg)_2(Si_4O_{10})(OH)_2.nH2O$ and CEC of 0.92 meq/g) was supplied by Sigma-Aldrich and Southern-Clay Products, USA,

respectively. FMT powder was obtained by Hakim Pharmaceutical Company. NaOH, HCl, KH2PO4, acetic acid, and sodium tripolyphosphate (STTP) were supplied from Merck and used without any further purification. Bi-distilled water was used in all experiments.

3.2. Preparation of MMT-FMT Particles

MMT-FMT particles were prepared using an ion exchange process in accordance with the following prescribed conditions (optimized conditions):

First, MMT dispersion was prepared by adding 400 mg of MMT to 50 mL of bi-distilled water and stirring for 2 hours. In order to get a homogenous dispersion, the dispersion was sonicated in a sonication bath for 20 minutes at 25°C. Then, 50 mL of FMT solution (0.024M) was added to the MMT dispersion and constantly stirred at room temperature. Finally, the pH of the mixture was adjusted to 5.8 by hydrochloric acid (0.1N) and sodium hydroxide (0.1N) solutions. Next, for the incorporation of FMT into the nano-space between layers of MMT, the mixture was incubated for 5 hours at ambient temperature. Subsequently, the dispersion was centrifuged at 3000 rpm, and the participated MMT-FMT particles were washed 3 times with double distilled water to remove the un-trapped drug molecules. After vacuuming for 24 hours at 50°C, the obtained MMT-FMT particles were powdered via a mortar and pestle set, sieved using a 180-micron mesh sieve, and kept in a desiccator.

3.3. Drug Loading Analysis

To measure the content of FMT incorporated into the nano-space between layers of MMT-FMT particles, the dispersion containing both unreacted FMT and MMT-FMT particles was centrifuged, and the supernatant was collected and filtered with a 0.45-micron sterile syringe filter (SF-PVDF030045SL) and analyzed using an ultraviolet-visible (UV-vis) spectroscopy at a wavelength of 266 nm. The content of FMT incorporated into the nano-space between layers of MMT-FMT particles was obtained by subtracting the amount analyzed by UV-vis from the initial amount that was introduced to the dispersion. The percentage of drug loading (DL%) of MMT-FMT particles was measured according to Equation 1. The content of FMT loaded in MMT-FMT particles was 33.33 wt %.

$$Drug\ Loading\ Percentage\ (DL\%) = \frac{Weight\ of\ FMT\ loaded\ into\ nanohybrid\ (mg)}{Weight\ of\ Mt-FMT\ nanohybrid\ (mg)} \times 100 \quad (1)$$

3.4. Fabrication of MMT-FMT/CH Bio-nanocomposite Hydrogels

The extended-release profile of FMT was acquired by incorporating the resultant MMT-FMT particles into CH hydrogels. To fabricate MMT-FMT/CH bio-nanocomposite hydrogels, we applied an ionotropic gelation technique reported via Yadollahi et al. (31). Two grams of CH polymer was added to 40 mL of bi-distilled water containing 2.5 mL of acetic acid and stirred at 500 rpm for 12 hours to get a uniform viscous solution. A suitable amount of powder (900 mg MMT-FMT particles), which contained 300 mg FMT, was added to 20 mL of bi-distilled water, stirred for 10 minutes, sonicated for 40 minutes, and gradually added to the CH polymeric solution. The resultant dispersion was again stirred for 3 hours at 25°C to make it completely homogeneous. Next, the resultant homogeneous dispersion was injected in the form of droplets by a 23-gauge needle and a peristaltic pump into a 400-mL aqueous solution containing 4 g of TPP at 25°C under constant stirring (50 rpm). The falling distance and pumping rate are 2 cm and 20 mL/h, respectively. The fabricated bio-nanocomposite hydrogels were solidified into the TPP solution for 1 hour and collected via filtration. Then, the resultant bio-nanocomposite hydrogels were washed with 1 L of bi-distilled water and freeze-dried. Also, we used this method to fabricate FMT/CH hydrogels.

3.5. Characterization

The morphology of MMT-FMT/CH bio-nanocomposite hydrogels was evaluated using a scanning electron microscope (SEM; KYKY-SEM-3200) at a voltage of 26 kV. Interactions between MMT, FMT, and CH in test samples and their structure were evaluated by a Fourier-transform infrared spectrophotometer (FTIR; Thermo-Nicolet NEXUS-670 FTIR). Their FTIR spectra were recorded using the KBr pellet technique at 400-4000 cm-1 and a resolution of 0.5 cm^{-1}. The thermal behavior of these samples was recorded via the TGA-50H thermogravimetric device at 25 - 1000°C. The heating rate was 10°C/min, and the nitrogen flow rate was kept at 20 mL/min. X-ray diffraction (XRD) analysis of test samples was carried out with the STOE-STADI powder diffractometer system with Cu-K (λ = 1.54060°A). The instrument was operated in the 2θ range of 2°-50°, 40 kV, and 40 mA.

3.6. Swelling Profile Analysis

There are different cations and anions in the GI tract, which can have a remarkable influence on the swelling and drug release behaviors of MMT-FMT/CH bio-nanocomposite hydrogels. Thus, their swelling profile was investigated at different pHs. To study their swelling profile, 1 g of MMT-FMT/CH bio-nanocomposite hydrogels was

immersed in different buffer solutions at 25°C for 10 hours. Before weighing, the water on their surface was eliminated by blotting with filter paper. Finally, the swelling degree of MMT-FMT/CH bio-nanocomposite hydrogels was calculated using Equation 2:

$$Swelling\ Gegree\ (SD\%) = \frac{W_2 - W_1}{W_1} \times 100 \quad (2)$$

Where W_1 is the initial mass of samples, and W_2 is the mass of swollen gels. All tests were performed 3 times, and data were recorded as mean ± SD.

3.7. Drug Encapsulation Efficacy Analysis

The encapsulation efficacy (EE%) of MMT-FMT/CH bio-nanocomposite hydrogels was examined based on a method reported in our previous study (8). That is, 200 mg of the crushed and grounded MMT-FMT/CH bio-nanocomposite hydrogels were suspended in 40 mL acid buffer (pH = 1.2), sonicated for 20 minutes, and incubated at 37°C for 12 hours. The resultant suspension was filtered and washed twice with 30 mL of acid buffer. Finally, the FMT amount of the resultant solution was determined using a UV-vis spectrophotometer. The encapsulation efficacy (EE%) of bio-nanocomposite hydrogels was determined by Equation 3:

$$Encapsulation\ Efficiency\ (EE\%) = \frac{W_2}{W_1} \times 100 \quad (3)$$

Where W_2 and W_1 are the actual and theoretical FMT masses in the fabricated bio-nanocomposite hydrogels, respectively.

3.8. Mucoadhesive Property Analysis

A rather ordinary designed apparatus, which possessed 2 platforms arranged on a vertical axis with adjustable spacing between them, was applied to measure the mucoadhesive property of MMT-FMT/CH bio-nanocomposite hydrogels. New sheep gastric mucosal tissue was obtained and kept frozen in phosphate-buffered saline (PBS) pH 6.8 until the experiment time. Before conducting the tests, the mucosal tissue was allowed to reach the ambient temperature. In each experiment, MMT-FMT/CH bio-nanocomposite hydrogels (20 spherical hydrogels) were stocked to the top platform via double-sided adhesive tape. Next, a part of the stomach mucosal tissue was adhered to the bottom platform and immersed in the buffer solution. Subsequently, the top platform with the stocked hydrogels was lowered to get in contact with the tissue. Then, the bottom platform was gently moved down at a speed of 1 mm min^{-1} until the MMT-FMT/CH bio-nanocomposite hydrogels were detached from mucosal tissue. The maximum required force to detach the top platform with the hydrogels adhered from the stomach mucosal tissue was recorded as the mucoadhesive property of the fabricated bio-nanocomposite hydrogels. Each measurement was done in triplicate, and the mean values were reported.

3.9. Drug Release Profile Analysis

An in vitro drug release analysis for FMT from MMT-FMT/CH bio-nanocomposite hydrogels was performed in simulated gastric fluid (SGF, pH 1.2) for 12 hours. Thus, we used drug dissolution apparatus II USP (Paddle, Kavosh Co, Iran). The desired quantity of MMT-FMT/CH bio-nanocomposite hydrogels and MMT-FMT particles containing 300 mg of FMT was suspended in 5 mL of SGF in dialysis tubing (molecular weight cut-off of 12 kDa). Then, dialysis tubing containing test samples was placed in 0.9 L of the same SGF solution and kept at 37 ± 0.5°C under a stirring rate of 50 rpm. At certain times, 5-mL aliquots were removed from the dissolution medium, and the new SGF solution was added to it. FMT content of the removed samples was measured via UV-vis spectrophotometry at a wavelength of 266 nm. Measurements were carried out in triplicate for each sample, and results were reported as average ± SD.

3.10. Drug Release Kinetics Study

To assess the drug release kinetics, an in vitro release of the FMT from MMT-FMT/CH bio-nanocomposite hydrogels in SGF (pH 1.2) was fitted to various mathematical models, such as zero-order (Equation 4), first-order (Equation 5), Higuchi (Equation 6), and Korsmeyer–Peppas (Equation 7).

$$f_t = K_0 t \quad (4)$$

$$ln\,(1 - f_t) = k_1 t \quad (5)$$

$$f_t = k_H t^{\frac{1}{2}} \quad (6)$$

$$f_t\ = k_p t^n\ (ln f_t = ln k_p + n ln t) \quad (7)$$

Where f_t, t, k_P, and k0, k1, and k_H are attributed to the amount of the drug released at t, release time, rate constant, and rate constants of zero-order, first-order, and Higuchi models, respectively; n is the release exponent, indicating the release mechanism of FMT from these bio-nanocomposite hydrogels. For spherical hydrogels, $n \leq 0.43$, $43 < n < 85$, and $n \geq 0.85$ are indicative of Fickian release (diffusion-controlled drug release), non-Fickian release (diffusion and swelling-controlled drug releases), and case-II transport (polymer relaxation-dissolution), respectively (8).

4. Results and Discussion

4.1. Fabrication of MMT-FMT/CH Bio-nanocomposite Hydrogels

CH is a bioadhesive cationic polysaccharide that can be physically cross-linked by electrostatic interactions with TPP anions due to the presence of amino functional groups in its structure (31). Therefore, adding a dispersion of CH and MMT-FMT particles dropwise to the TPP solution leads to cross-linking of the CH macromolecules and the formation of spherical MMT-FMT/CH bio-nanocomposite hydrogels. Figure 1 shows how to make spherical MMT-FMT/CH bio-nanocomposite hydrogels as gastroretentive/mucoadhesive drug delivery systems.

4.2. Characterization of MMT-FMT/CH Bio-nanocomposite Hydrogels

4.2.1. FTIR Analysis

Figure 2 displays the results obtained from the FTIR analysis of FMT, MMT nanoclay, MMT-FMT nanohybrid, CH, TPP–cross-linked CH beads, and MMT-FMT/CH nanocomposite hydrogel beads. As can be seen in Figure 2, the pure FMT powder had characteristic peaks at 2900 - 3200 cm^{-1} (aromatic and aliphatic C–H stretching vibration), 3500 cm^{-1} (N–H antisymmetric stretching vibration), 3400 cm^{-1} (N–H symmetric stretching vibration), 1650 cm^{-1} (N–H bending vibration), and 1150 cm^{-1} (C–N stretching vibration) (50). In the results obtained from the FTIR analysis of MMT nanoclay, the peaks related to the stretching and bending vibrations of M–OH and stretching vibrations of M–O were observed in the wavenumber ranges of 3500 - 3600, 400 - 600, and 1000 - 1100 cm^{-1}, respectively. Also, peaks that appeared in the wavenumbers of 3400 and 1600 cm^{-1} may be caused by the OH stretching and bending vibrations of water molecules trapped in the nano-space between the layers of MMT nanoclay, respectively (53). The results obtained from the FTIR analysis of the MMT-FMT particles indicated peaks in the wavenumber ranges of 400 - 600 and 1000 - 1100 cm^{-1}, which attributed to M–OH bending and M–O stretching vibrations of montmorillonite (Mt) nanoclay, respectively. These results indicate that there is no intervention with the inherent properties of MMT nanoclay because of the incorporation of FMT. Moreover, the lack of characteristic FMT peaks in the wavenumber ranges of 1150, 1400 - 1600, and 2900 - 3200 cm^{-1} is indicative of the high incorporation of FMT into the nano-space between layers of MMT particles. Moreover, bands with a low intensity appearing at 3000, 2900, 1600, and 1400 cm^{-1} are due to the FMT incorporated into MMT-FMT particles, indicating the adsorption of a very small amount of FMT on MMT particles. From the results obtained in this paragraph, it can be said that the drug FMT was effectively incorporated into the nano-space between the layers of MMT particles; thus, the synthesis of MMT-FMT particles was successful. These results are in agreement with similar data reported in the literature (54).

FTIR spectrophotometer was also used to evaluate the prepared MMT-FMT/CH bio-nanocomposite hydrogels. The results obtained from FTIR analysis showed that CH chains were cross-linked with TPP anions (cross-linking agent). This phenomenon can be because of the existence of high ionic bonding between TPP anions and amines of the CH chains. The results obtained from the FTIR analysis of the net CH polymer displayed a wide absorption peak at 3400 cm^{-1} because of the overlapped vibrations of NH_2 and OH stretching bands and inter- and intramolecular hydrogen bonding. Moreover, the peaks related to the stretching mode of CH and bending modes of amide and $–CH_2$ bending modes appeared in the wavenumbers 2900, 1640, and 1400 cm^{-1}, respectively. Also, the peaks at 1000 - 1200 cm^{-1} were because of the stretching vibration of cycloolefin copolymer (COC) in the structure of the CH polymer (55). The results obtained from the FTIR analysis of the TPP–cross-linked CH hydrogels indicated that the peak related to the overlapped vibrations of NH_2 and OH stretching bands was transferred from a higher wavenumber (3400 cm^{-1}) to a lower wavenumber (3300 cm^{-1}). Also, the intensity of this peak was significantly reduced. This phenomenon can be because of ionic interactions between amines of CH and TPP anions and cross-linking of CH matrix with TPP anions. Moreover, the peak of amide bending was shifted from 1640 cm^{-1} to a lower wavenumber (1620 cm^{-1}), and its intensity decreased due to the ionic interactions between TPP anions and amines of CH. Knaul et al. reported the same data in the project of CH matrix modified with sodium dihydrogen phosphate and related it to the electrostatic interaction between PO43- anions and NH_4^+ cations (56). Also, Xu and Du showed that in CH nanoparticles, NH_4^+ cations on CH chains interacted with TPP anions (57). In addition, a novel absorption band was observed at 1250 cm^{-1} because of the vibration of P = O stretching in TPP cross-linked CH beads, which is absent in the pure CH powder (58). The resultant data revealed that the ionic bonds between TPP anions and NH_4^+ cations of CH were created in the TPP–cross-linked CH hydrogel beads. In the data obtained from the FTIR analysis of TPP–cross-linked MMT-FMT/CH samples, peaks appeared in the wavenumber range of 500 - 900 cm^{-1} are due to the stretching vibrations of M–O of MMT-FMT particles, indicating the incorporation of MMT-FMT particles into TPP–cross-linked CH hydrogel beads and the formation of MMT-FMT/CH nanocomposite hydrogel beads. Therefore, it can be said that MMT-FMT/CH bio-nanocomposite hydrogels were created successfully.

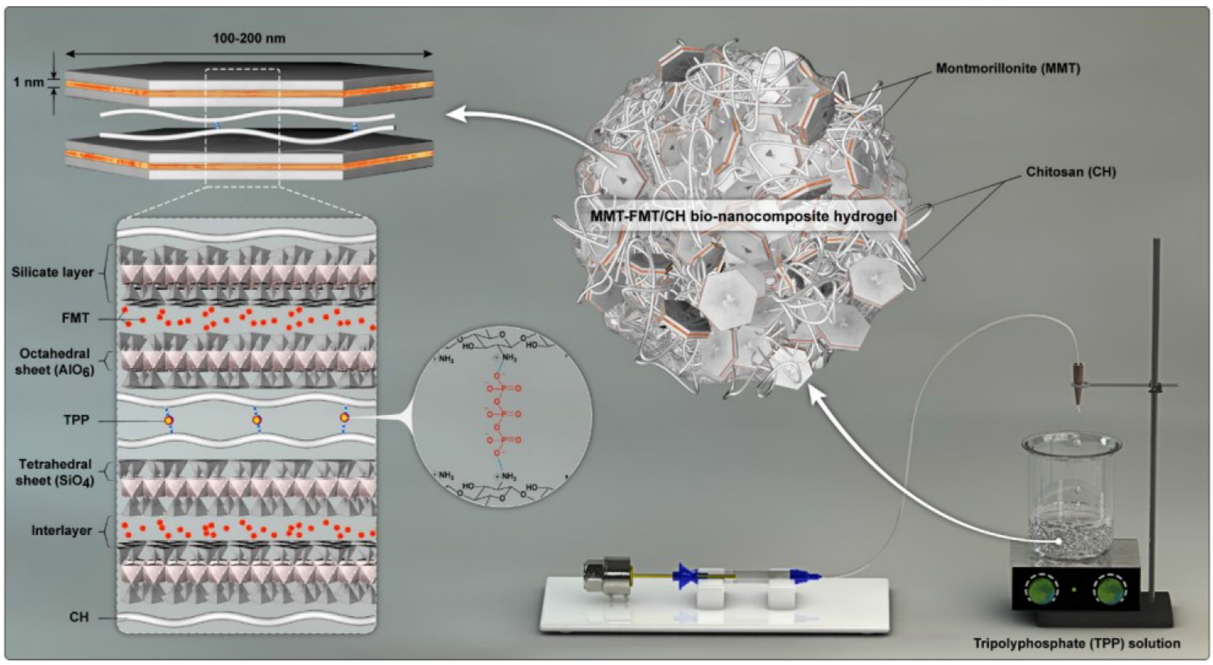

Figure 1. The formation of spherical MMT-FMT/CH bio-nanocomposite hydrogels as gastroretentive/mucoadhesive drug delivery systems

4.2.2. XRD Analysis

The XRD pattern of MMT nanoclay and MMT-FMT particles in the 2θ range of 1° - 50° is displayed in Figure 3. The diffractogram of MMT nanoclay showed a main peak at $2\theta = 7.4°$, which is attributed to d001-spacing (1.18 nm) of MMT nanoclay (59). For MMT-FMT particles, the characteristic diffraction peak attributed to the 001 plane shifted to a lower diffraction angle ($2\theta = 5.2°$). The d001-spacing of MMT-FMT particles was calculated based on the Bragg law, and it was 1.68 nm, indicating an enhancement in the d001-spacing of MMT-FMT particles compared to MMT nanoclay. This phenomenon obviously supported the introduction of the FMT drug into the nano-space between layers of MMT nanoclay. Thus, the results obtained from the XRD analysis showed that MMT-FMT particles were successfully created, as shown in Figure 4. Hydrogen and ionic bonds between the silicate layers of MMT nanoclay and FMT drug led to the introduction of FMT into nano-space between layers of MMT nanoclay. Similar reports regarding other drug-MMT nanohybrid particles have also been published in the literature (60, 61).

4.2.3. SEM Analysis

The morphological property of drug delivery systems is one of the most vital parameters significantly affecting its release profile. The existence of various interactions between CH chains and MMT-FMT particles can vary the morphological property of the MMT-FMT/CH bio-nanocomposite hydrogels, which have an evident influence on their release behavior. Thus, the morphological property of MMT-FMT/CH bio-nanocomposite hydrogels was examined. Figure 5 shows the digital images of MMT-FMT/CH bio-nanocomposite hydrogels in dry and wet states. As shown in Figure 5, the wet beads were spherical and smooth. After drying, their size slightly decreased but still had a spherical shape. A possible explanation for such a phenomenon is that H2O molecules in MTT-FMT/CH bio-nanocomposite hydrogels were evaporated in the drying step. Thus, the fabricated bio-nanocomposite hydrogels constricted, leading to a minor reduction in their sizes.

Figure 5 shows the SEM images of the TPP–cross-linked FMT/CH and MMT-FMT/CH bio-nanocomposite hydrogels. As shown in Figure 5, the surface of TPP–cross-linked FMT/CH hydrogels is rough, and many porosities and wrinkles are observed on their surface. However, the SEM images of the TPP–cross-linked MMT-FMT/CH bio-nanocomposite hydrogels displayed slight wrinkles on the smooth surface of these bio-nanocomposite hydrogels. A possible description of this phenomenon could be that different interactions between CH macromolecules and MMT-FMT particles resulted in changes in their morphological properties. Also, the SEM images of the TPP–cross-linked MMT-FMT/CH nanocomposite bead confirmed the existence of MMT-FMT nanohybrid particles on their sur-

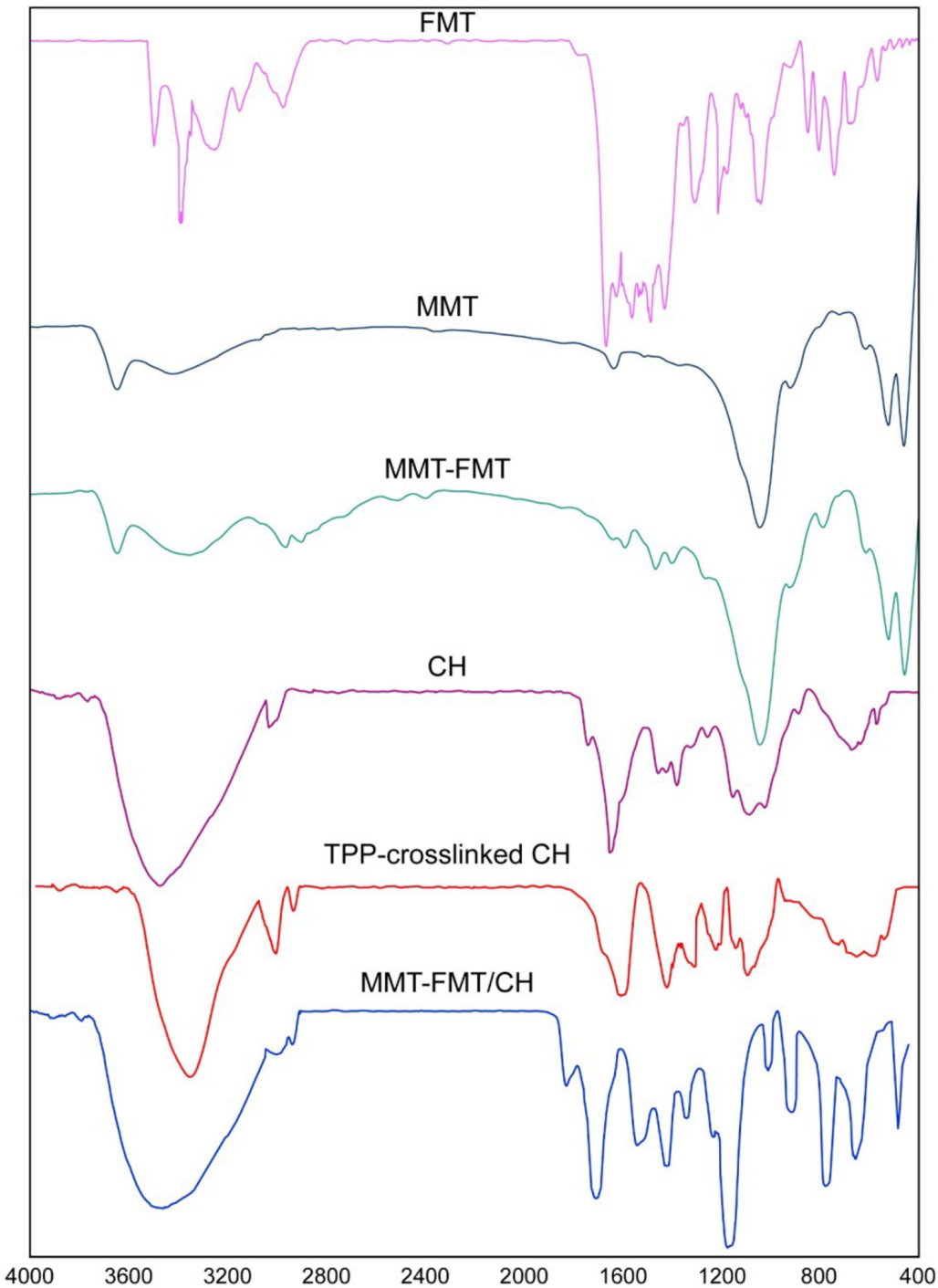

Figure 2. Fourier-transform infrared spectroscopy spectra of test samples

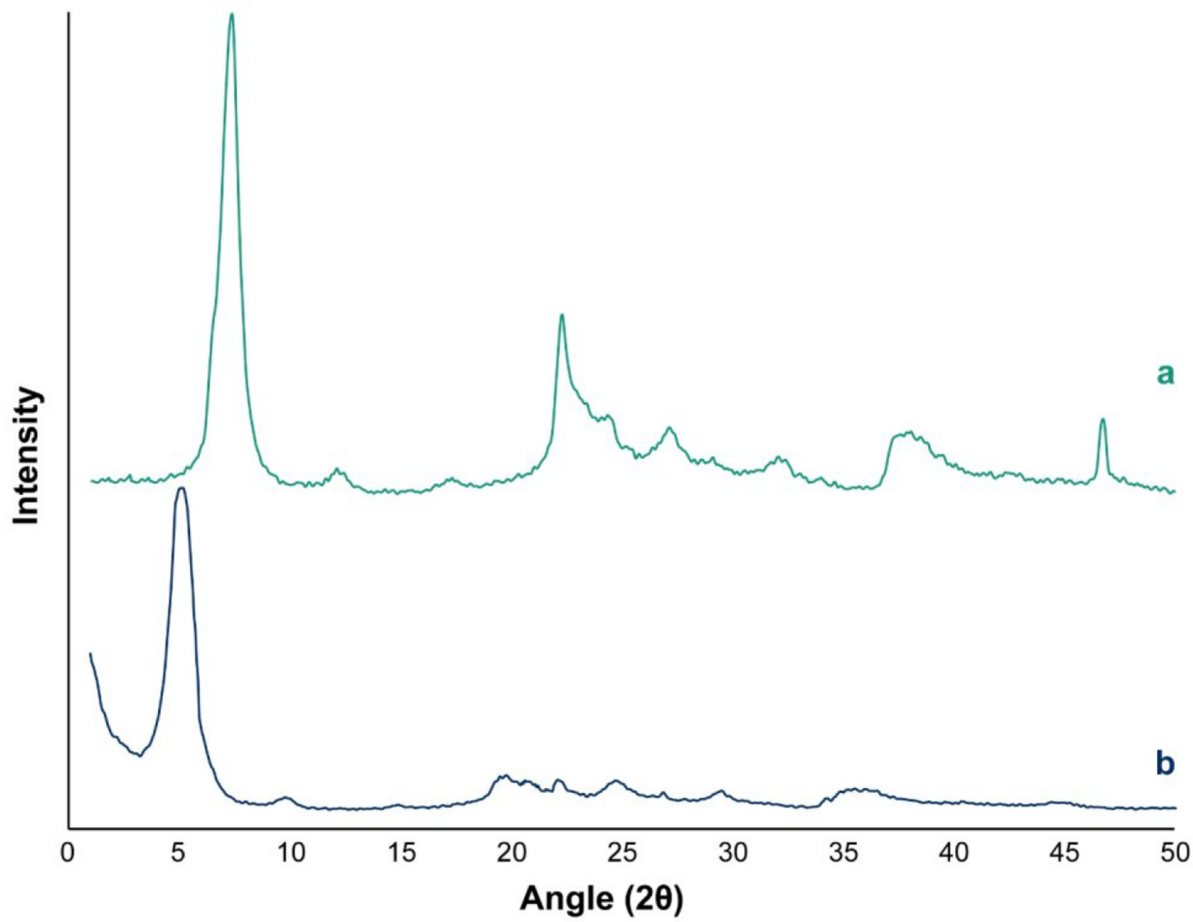

Figure 3. The results obtained from the XRD analysis of A, MMT nanoclay; and B, MMT-FMT particles

faces, and the MMT-FMT nanohybrid particles were well dispersed in the CH matrix.

4.2.4. TGA Analysis

Figure 6 shows the thermal behavior of FMT, MMT nanoclay, CH powder, MMT-FMT particles, and MMT-FMT/CH bio-nanocomposite hydrogels. As shown in Figure 6, neat FMT powder showed 2 main mass loss phases in the temperature ranges of 170 - 270 and 360 - 750°C due to its thermal decomposition (62). The TGA curve of MMT nanoclay presented a mass loss at 540 - 630°C that might be because of the miss of OH functional groups in its structure (8). Also, 2 mass loss phases were observed at 230 - 460°C and 550 - 650°C for MMT-FMT particles, which could be because of the destruction of incorporated FMT molecules and the miss of OH functional groups in the structure of MMT-FMT particles, respectively. The results obtained from the TGA curve of Mt-FMT nanohybrid particles showed that destruction T of FMT molecules in the MMT-FMT particles moves to higher T compared to the neat FMT, confirming the incorporation of FMT drugs into the nano-space between layers of MMT nanoclay. The TGA curve of the CH showed 2 mass loss phases in the temperature ranges of 230 - 330 and 330 - 590°C, which could be because of the destruction of CH chains and the creation of carbon residues, respectively (63). There was also a slight mass loss in T below 110°C, which might be because of the miss of water molecules adsorbed on the surface of CH chains. The TGA curve of MMT-FMT/CH bio-nanocomposite hydrogels showed 4 mass loss phases at 80 - 100, 300 - 380, 390 - 520, and 510 - 660°C. The first mass loss in the range of 80 - 100°C was due to the evaporation of water molecules adsorbed on their surfaces. The second and third mass losses (300 - 380 and 390 - 520°C) were related to the degradation of FMT molecules and deacetylation of CH chains, and the fourth mass loss (510 - 660°C) was caused by the loss of Mt's structural hy-

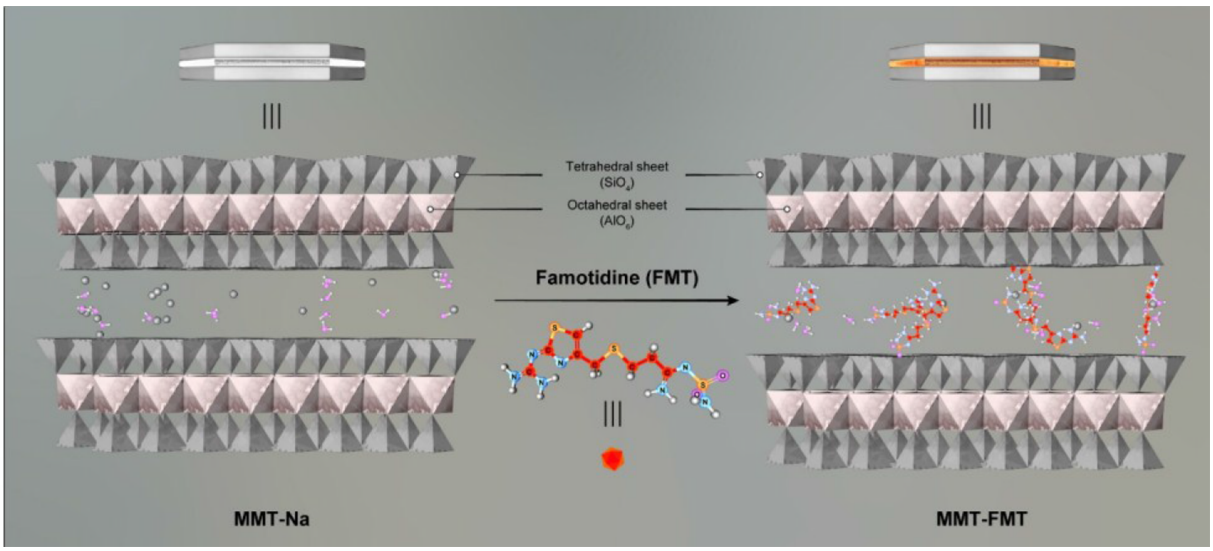

Figure 4. The incorporation of FMT molecules into the nano-space between layers of MMT nanoclay using an ion-exchange technique

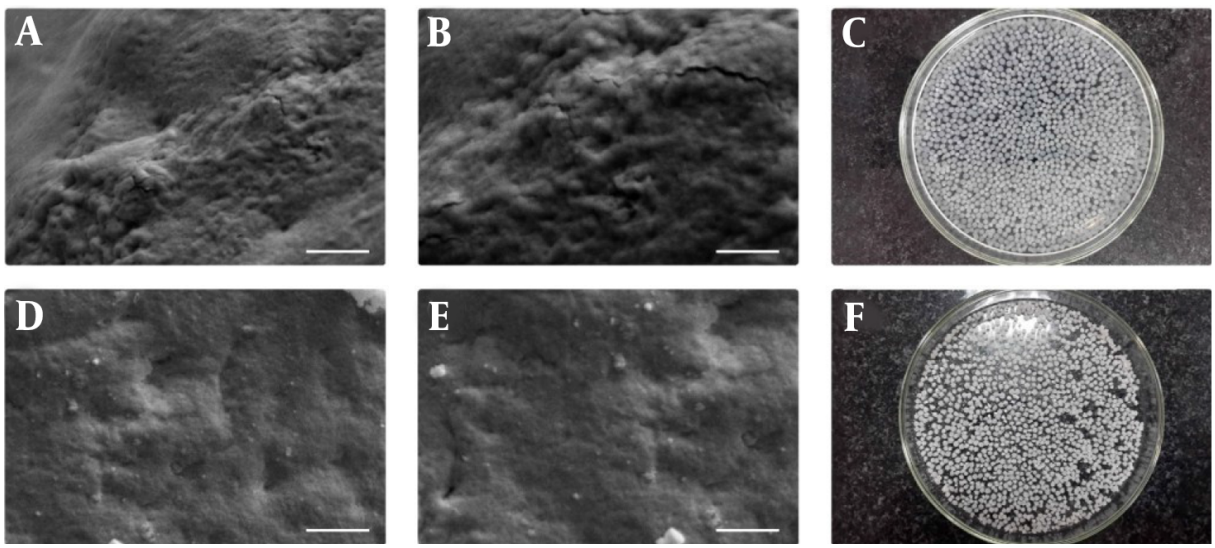

Figure 5. The SEM images of TPP-cross-linked FMT/CH (A and C); MMT-FMT/CH bio-nanocomposite hydrogels (B and D); and the digital images of MMT-FMT/CH bio-nanocomposite hydrogels [wet (e) and dry (f)]

droxyl functional groups, the degradation of species derived from the deacetylation of CH chains, and the formation of carbon residues. Also, the TGA curve of MMT-FMT/CH bio-nanocomposite hydrogels showed that their mass loss shifted to a higher T (300°C) compared to that of the neat CH, confirming the existence of MMT nanoclay in the hydrogel matrix and the interactions between CH chains and TPP anions, which led to the enhancement of the thermal stability of MMT-FMT/CH bio-nanocomposite hydrogels.

4.3. Swelling Behavior Analysis

The swelling behavior of MMT-FMT/CH bio-nanocomposite hydrogels at various pHs and MMT nanoclay amounts was investigated, and the data are given in Figure 7. As shown in Figure 7, the swelling degree of test bio-nanocomposite hydrogels increased rapidly with time and then slowly until it reached a steady state

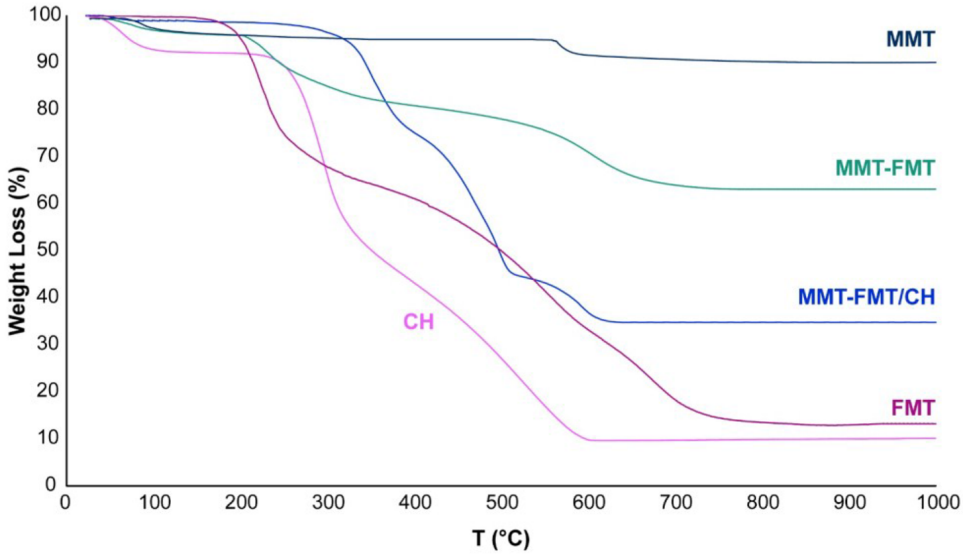

Figure 6. TGA curves of the samples

(equilibrium). Also, Figure 7 shows that the swelling degree of the fabricated bio-nanocomposite hydrogels is enhanced by decreasing the amount of pH because, at acidic pH, the amino groups of CH protonated in the swelling medium and converted to NH_4^+ cations, which resulted in stronger electrostatic repulsion force between CH macromolecules and consequently more water penetration into the fabricated bio-nanocomposite hydrogels (64). The influence of MMT nanoclay on the swelling behavior of the fabricated bio-nanocomposite hydrogels was examined. It is clear from Figure 7 that MMT-FMT/CH bio-nanocomposite hydrogels had a lower swelling degree than FMT/CH hydrogels. In addition, their swelling degree was reduced by enhancing MMT nanoclay content in bio-nanocomposite hydrogels. Such behavior can be related to the role of MMT nanoclay as a chelating agent that prevents the expansion of CH chains (8).

4.4. Drug Incorporation Efficacy Analysis

The drug incorporation efficacy of the TPP–cross-linked MMT-FMT/CH bio-nanocomposite hydrogels ranged from 37.6 to 84.5 (Table 1), depending on their composition. The drug incorporation efficacy of the TPP–cross-linked MMT-FMT/CH bio-nanocomposite hydrogels was enhanced by increasing the content of MMT nanoclay. There are two major causes for such behavior (8): (1) the formation of MMT-FMT particles in the dispersion before the cross-linking reaction, leading to the enhancement of the drug incorporation efficacy; and (2) the existence of interactions between MMT and CH macromolecules led to the inhibition of FMT leakage during the formation of the TPP–cross-linked Mt-FMT/CH nanocomposite beads.

Table 1. Drug Encapsulation Efficiency (%) and Mucoadhesive Strength (g) of the Test Samples

Sample Names	Drug Encapsulation Efficiency (%)	Mucoadhesive Strength (g)
FMT/CH	37.6 ± 3.1	41.5 ± 4.2
Mt1-FMT/CH	57.2 ± 4.8	39.7 ± 3.3
Mt2-FMT/CH	67.8 ± 6.3	37.4 ± 3.8
Mt3-FMT/CH	84.5 ± 5.9	38.7 ± 2.9

4.5. Mucoadhesive Property Analysis

The data obtained from the analysis of the mucoadhesive property of the FMT/CH hydrogel and MMT-FMT/CH bio-nanocomposite hydrogels are presented in Table 1. This study showed that the test beads possessed a high mucoadhesive property. One possible elucidation for such a phenomenon could be that test beads are positively charged due to having amino functional groups, which can interact with the mucus on the outer wall of the stomach (which is negatively charged), indicating the existence of a strong interaction between the test beads and gastric mucosal tissue. This property enables the fabricated beads to stick to the mucosal surface of the stomach and stay in it for a long time, which can guarantee the stability of FMT in the SGF medium, leading to superior bioavailability at much lower doses (3, 18). Also, Table 1 shows that the mucoad-

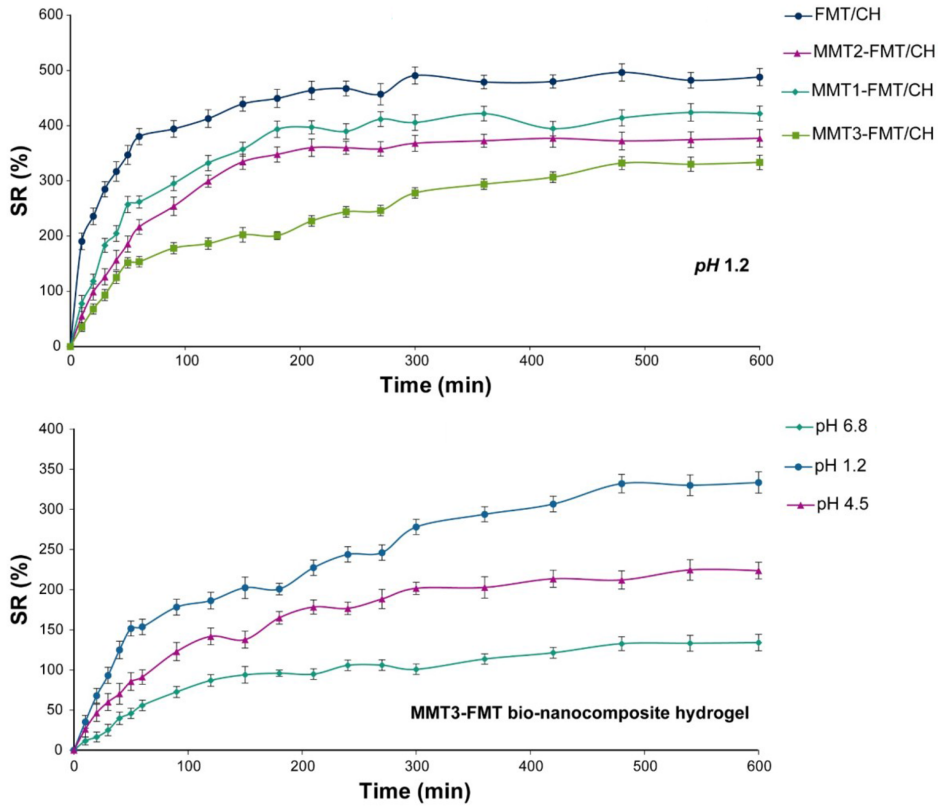

Figure 7. The swelling behavior of the test samples

hesive strength of the FMT/CH hydrogel and MMT-FMT/CH bio-nanocomposite hydrogels are almost the same. This phenomenon indicates that the existence of MMT-FMT particles in the fabricated bio-nanocomposite hydrogels does not affect their mucoadhesive strength.

4.6. In Vitro Drug Release Analysis

The release profile of FMT from the FMT and MMT physical mixture, MMT-FMT particles, FMT/CH hydrogel, and MMT-FMT/CH bio-nanocomposite hydrogels was evaluated in the SGF medium (pH 1.2), and the data are given in Figure 8. As shown in Figure 8, the physical mixture of Mt and FMT displayed a rapid release of about 100% of FMT in the release medium in the initial 60 minutes because FMT dissolves rapidly in the SGF medium (pH 1.2) due to its protonation ability. Significant differences between the drug release profiles of the physical mixture of MMT and FMT, MMT-FMT particles, FMT/CH hydrogel, and MMT-FMT/CH bio-nanocomposite hydrogels were observed in the SGF medium (pH 1.2). As shown in Figure 8, the initial release content of FMT from the FMT/CH hydrogels was significantly more than that of MMT-FMT/CH bio-nanocomposite hydrogels in the SGF medium (pH 1.2). It is caused by the higher swelling degree of FMT/CH hydrogel beads in SGF (pH 1.2), which leads to the penetration of high amounts of H_2O into test beads, dissolving the incorporated FMT, and initial burst release of the drug into the SGF medium. Also, the introduction of MMT nanoclay into CH hydrogels extended the release of FMT from the fabricated bio-nanocomposite hydrogels. Such behavior is due to the existence of MMT nanoclay that prolonged the path taken by incorporating FMT into MMT-FMT/CH bio-nanocomposite hydrogels, resulting in more decrease in initial burst release and higher prolongation of the FMT release profile compared to FMT/CH hydrogels.

4.7. Release Kinetics Analysis

The release kinetics of FMT from MMT-FMT/CH bio-nanocomposite hydrogels was investigated according to the Korsmeyer-Peppas kinetic model, and data are presented in Table 2. As shown in Table 2, the amount of n for MMT-FMT/CH bio-nanocomposite hydrogels in the SGF medium was 0.62. This indicates that the release of FMT from the test beads in an SGF medium is controlled by both

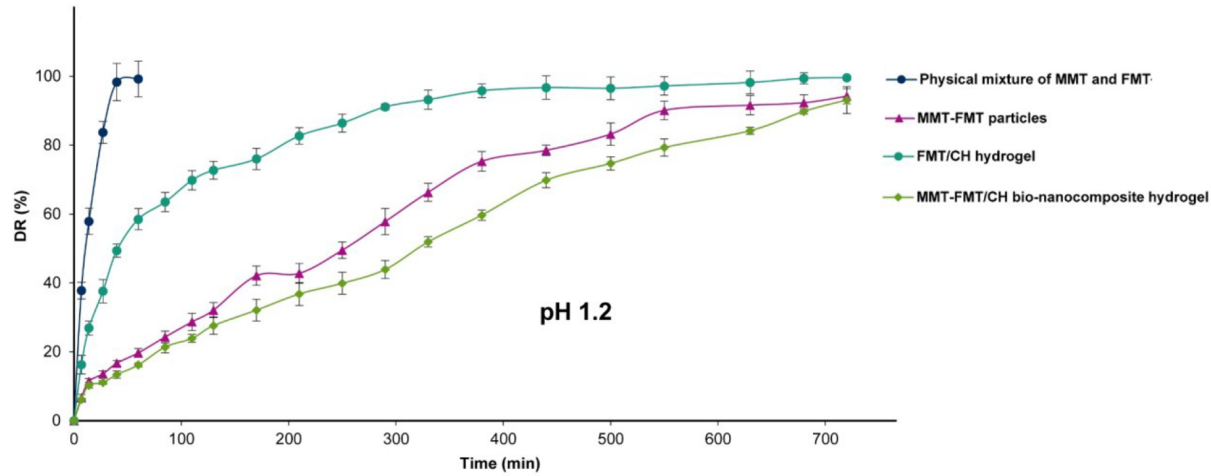

Figure 8. The release profile of FMT from the FMT and MMT physical mixture, MMT-FMT particles, FMT/CH hydrogel, and MMT-FMT/CH bio-nanocomposites hydrogels

the diffusion and swelling processes (non-Fickian transport). Also, the drug release data from MMT-FMT/CH bio-nanocomposite hydrogels was studied kinetically by different mathematical models (zero-order, first-order, and Higuchi). As it is clear from Table 2, the FMT release kinetics of MMT-FMT/CH bio-nanocomposite hydrogels conforms to the Higuchi model because the amount of the correlation coefficient of the Higuchi model (R_H^2) is closer to 1 compared to that of R_0^2 and R_1^2.

Table 2. Kinetic Model Factors of MMT-FMT/CH Bio-nanocomposite Hydrogels

Kinetic Model Parameters	MMT-FMT/CH Bio-nanocomposite Hydrogels
n	0.62
R_0^2	0.99
R_1^2	0.97
R_H^2	0.95

Abbreviations: n, kinetic exponent; R^2: regression coefficient.

5. Conclusion

In this project, we successfully fabricated novel mucoadhesive and pH-responsive MMT-FMT/CH bio-nanocomposite hydrogels by the dispersion of MMT-FMT particles into the CH hydrogel, followed by a cross-linking via TPP anions as a mucoadhesive/gastroretentive drug carrier. The fabrication method was modest, reproducible, and inexpensive. The physiochemical characterization of MMT-FMT/CH bio-nanocomposite hydrogels showed the presence of strong interactions between the polymeric matrix and FMT, TPP anions, and MMT nanoclay. The SEM analysis showed that the surface of the fabricated MMT-FMT/CH bio-nanocomposite hydrogels was smooth. Increasing the amount of MMT nanoclay into CH hydrogels resulted in a notable enhancement of the thermal stability of the fabricated bio-nanocomposite hydrogels, as well as a remarkable reduction of their swelling degree, initial burst release, and release rate. In addition, the release of FMT from the test bio-nanocomposite hydrogels was pH-dependent due to the CH. MMT-FMT/CH bio-nanocomposite hydrogels showed an extended release of FMT for up to 12 hours compared to FMT/CH hydrogels. In addition, the test bio-nanocomposite hydrogels displayed good and strong mucoadhesion and gastroretentive properties. Our study indicates that fabricated bio-nanocomposite hydrogels might be applied as a suitable carrier for oral delivery of FMT to modify its bioavailability and prolong its retention time in the stomach.

Footnotes

Authors' Contribution: Study concept and design: S. A. M., and H. F.; Acquisition of data: H. F., H . M., and A. M.; analysis and interpretation of data: H. F., S. A., A. R., and H. M.; drafting of the manuscript: H. F., and Y. F.; critical revision of the manuscript for important intellectual content: S. A. M., H. F., and Y. F.; statistical analysis: B. D., A. M.

Conflict of Interests: The authors declare that they have no known competing financial interests or personal relationships that could have appeared to influence the work reported in this paper.

Data Reproducibility: The dataset presented in the study is available on request from the corresponding author during submission or after its publication. The data are not publicly available due to preparing and developing a patent in future.

Funding/Support: This study was supported in part by grant 7291 from the Shahid Beheshti University of Medical Sciences and by a teaching and research scholarship from the Faculty of Pharmacy, Shahid Beheshti University of Medical Sciences, Tehran, Iran.

References

1. Sosnik A, Augustine R. Challenges in oral drug delivery of antiretrovirals and the innovative strategies to overcome them. *Adv Drug Deliv Rev*. 2016;**103**:105–20. doi: 10.1016/j.addr.2015.12.022. [PubMed: 26772138].
2. Darbasizadeh B, Motasadizadeh H, Foroughi-Nia B, Farhadnejad H. Tripolyphosphate-crosslinked chitosan/poly (ethylene oxide) electrospun nanofibrous mats as a floating gastro-retentive delivery system for ranitidine hydrochloride. *J Pharm Biomed Anal*. 2018;**153**:63–75. doi: 10.1016/j.jpba.2018.02.023. [PubMed: 29462781].
3. Lopes CM, Bettencourt C, Rossi A, Buttini F, Barata P. Overview on gastroretentive drug delivery systems for improving drug bioavailability. *Int J Pharm*. 2016;**510**(1):144–58. doi: 10.1016/j.ijpharm.2016.05.016. [PubMed: 27173823].
4. Hooda A, Nanda A, Jain M, Kumar V, Rathee P. Optimization and evaluation of gastroretentive ranitidine HCl microspheres by using design expert software. *Int J Biol Macromol*. 2012;**51**(5):691–700. doi: 10.1016/j.ijbiomac.2012.07.030. [PubMed: 22903013].
5. Rouge N, Buri P, Doelker E. Drug absorption sites in the gastrointestinal tract and dosage forms for site-specific delivery. *Int J Pharm*. 1996;**136**(1-2):117–39. doi: 10.1016/0378-5173(96)85200-8.
6. Kagan L, Hoffman A. Selection of drug candidates for gastroretentive dosage forms: pharmacokinetics following continuous intragastric mode of administration in a rat model. *Eur J Pharm Biopharm*. 2008;**69**(1):238–46. doi: 10.1016/j.ejpb.2007.10.019. [PubMed: 18068342].
7. Sarparanta MP, Bimbo LM, Makila EM, Salonen JJ, Laaksonen PH, Helariutta AM, et al. The mucoadhesive and gastroretentive properties of hydrophobin-coated porous silicon nanoparticle oral drug delivery systems. *Biomaterials*. 2012;**33**(11):3353–62. doi: 10.1016/j.biomaterials.2012.01.029. [PubMed: 22285465].
8. Farhadnejad H, Mortazavi SA, Erfan M, Darbasizadeh B, Motasadizadeh H, Fatahi Y. Facile preparation and characterization of pH sensitive Mt/CMC nanocomposite hydrogel beads for propranolol controlled release. *Int J Biol Macromol*. 2018;**111**:696–705. doi: 10.1016/j.ijbiomac.2018.01.061. [PubMed: 29337099].
9. Gerard DE, Schoelkopf J, Gane PA, Eberle VA, Alles R, Puchkov M, inventors. Gastroretentive drug formulation and delivery systems and their method of preparation using functionalized calcium carbonate. *USA*. 2018 5th Jun 2018.
10. Vashisth P, Raghuwanshi N, Srivastava AK, Singh H, Nagar H, Pruthi V. Ofloxacin loaded gellan/PVA nanofibers - Synthesis, characterization and evaluation of their gastroretentive/mucoadhesive drug delivery potential. *Mater Sci Eng C Mater Biol Appl*. 2017;**71**:611–9. doi: 10.1016/j.msec.2016.10.051. [PubMed: 27987752].
11. Singh H, Sharma R, Joshi M, Garg T, Goyal AK, Rath G. Transmucosal delivery of Docetaxel by mucoadhesive polymeric nanofibers. *Artif Cells Nanomed Biotechnol*. 2015;**43**(4):263–9. doi: 10.3109/21691401.2014.885442. [PubMed: 24621011].
12. Biswas N, Sahoo RK. Tapioca starch blended alginate mucoadhesive-floating beads for intragastric delivery of Metoprolol Tartrate. *Int J Biol Macromol*. 2016;**83**:61–70. doi: 10.1016/j.ijbiomac.2015.11.039. [PubMed: 26592698].
13. Raza A, Hayat U, Wang HJ, Wang JY. Preparation and evaluation of captopril loaded gastro-retentive zein based porous floating tablets. *Int J Pharm*. 2020;**579**:119185. doi: 10.1016/j.ijpharm.2020.119185. [PubMed: 32112929].
14. Charoenying T, Patrojanasophon P, Ngawhirunpat T, Rojanarata T, Akkaramongkolporn P, Opanasopit P. Fabrication of floating capsule-in- 3D-printed devices as gastro-retentive delivery systems of amoxicillin. *J Drug Deliv Sci Technol*. 2020;**55**:101393. doi: 10.1016/j.jddst.2019.101393.
15. Lemieux M, Gosselin P, Mateescu MA. Carboxymethyl starch mucoadhesive microspheres as gastroretentive dosage form. *Int J Pharm*. 2015;**496**(2):497–508. doi: 10.1016/j.ijpharm.2015.10.027. [PubMed: 26456246].
16. Sankar R, Jain SK. Development and characterization of gastroretentive sustained-release formulation by combination of swelling and mucoadhesive approach: a mechanistic study. *Drug Des Devel Ther*. 2013;**7**:1455–69. doi: 10.2147/DDDT.S52890. [PubMed: 24348022]. [PubMed Central: PMC3857114].
17. Mahalingam R, Jasti B, Birudaraj R, Stefanidis D, Killion R, Alfredson T, et al. Evaluation of polyethylene oxide compacts as gastroretentive delivery systems. *AAPS PharmSciTech*. 2009;**10**(1):98–103. doi: 10.1208/s12249-008-9182-1. [PubMed: 19148757]. [PubMed Central: PMC2663672].
18. Vasir JK, Tambwekar K, Garg S. Bioadhesive microspheres as a controlled drug delivery system. *Int J Pharm*. 2003;**255**(1-2):13–32. doi: 10.1016/s0378-5173(03)00087-5. [PubMed: 12672598].
19. Bardonnet PL, Faivre V, Pugh WJ, Piffaretti JC, Falson F. Gastroretentive dosage forms: overview and special case of Helicobacter pylori. *J Control Release*. 2006;**111**(1-2):1–18. doi: 10.1016/j.jconrel.2005.10.031. [PubMed: 16403588].
20. Mandal UK, Chatterjee B, Senjoti FG. Gastro-retentive drug delivery systems and their in vivo success: A recent update. *Asian J Pharm Sci*. 2016;**11**(5):575–84. doi: 10.1016/j.ajps.2016.04.007.
21. Bera H, Maiti S, Saha S, Nayak AK. Biopolymers-based gastroretentive buoyant systems for therapeutic management of Helicobacter pylori infection. In: Maiti S, Jana S, editors. *Polysaccharide Carriers for Drug Delivery*. Cambridge, UK: Woodhead Publishing; 2019. p. 713–36. doi: 10.1016/b978-0-08-102553-6.00024-6.
22. Lima DS, Tenório-Neto ET, Lima-Tenório MK, Guilherme MR, Scariot DB, Nakamura CV, et al. pH-responsive alginate-based hydrogels for protein delivery. *J Mol Liq*. 2018;**262**:29–36. doi: 10.1016/j.molliq.2018.04.002.
23. Carvalho SM, Mansur AA, Capanema NS, Carvalho IC, Chagas P, de Oliveira LCA, et al. Synthesis and in vitro assessment of anticancer hydrogels composed by carboxymethylcellulose-doxorubicin as potential transdermal delivery systems for treatment of skin cancer. *J Mol Liq*. 2018;**266**:425–40. doi: 10.1016/j.molliq.2018.06.085.
24. Ganguly R, Kumar S, Kunwar A, Nath S, Sarma HD, Tripathi A, et al. Structural and therapeutic properties of curcumin solubilized pluronic F127 micellar solutions and hydrogels. *J Mol Liq*. 2020;**314**:113591. doi: 10.1016/j.molliq.2020.113591.
25. Khan YA, Ozaltin K, Bernal-Ballen A, Di Martino A. Chitosan-alginate hydrogels for simultaneous and sustained releases of ciprofloxacin, amoxicillin and vancomycin for combination therapy. *J Drug Deliv Sci Technol*. 2021;**61**:102126. doi: 10.1016/j.jddst.2020.102126.
26. Jafari Z, Rad AS, Baharfar R, Asghari S, Esfahani MR. Synthesis and application of chitosan/tripolyphosphate/graphene oxide hydrogel as a new drug delivery system for Sumatriptan Succinate. *J Mol Liq*. 2020;**315**:113835. doi: 10.1016/j.molliq.2020.113835.
27. Lima-Tenório MK, Tenório-Neto ET, Garcia FP, Nakamura CV, Guilherme MR, Muniz EC, et al. Hydrogel nanocomposite based on starch and Co-doped zinc ferrite nanoparticles that shows magnetic

field-responsive drug release changes. *J Mol Liq*. 2015;**210**:100–5. doi: 10.1016/j.molliq.2014.11.027.
28. Ebrahimi MH, Samadian H, Davani ST, Kolarijani NR, Mogharabian N, Salami MS, et al. Peripheral nerve regeneration in rats by chitosan/alginate hydrogel composited with Berberine and Naringin nanoparticles: in vitro and in vivo study. *J Mol Liq*. 2020;**318**:114226. doi: 10.1016/j.molliq.2020.114226.
29. Siangsanoh C, Ummartyotin S, Sathirakul K, Rojanapanthu P, Treesuppharat W. Fabrication and characterization of triple-responsive composite hydrogel for targeted and controlled drug delivery system. *J Mol Liq*. 2018;**256**:90–9. doi: 10.1016/j.molliq.2018.02.026.
30. Pardeshi CV, Belgamwar VS. Controlled synthesis of N,N,N-trimethyl chitosan for modulated bioadhesion and nasal membrane permeability. *Int J Biol Macromol*. 2016;**82**:933–44. doi: 10.1016/j.ijbiomac.2015.11.012. [PubMed: 26562548].
31. Yadollahi M, Farhoudian S, Barkhordari S, Gholamali I, Farhadnejad H, Motasadizadeh H. Facile synthesis of chitosan/ZnO bionanocomposite hydrogel beads as drug delivery systems. *Int J Biol Macromol*. 2016;**82**:273–8. doi: 10.1016/j.ijbiomac.2015.09.064. [PubMed: 26433177].
32. Ali A, Ahmed S. A review on chitosan and its nanocomposites in drug delivery. *Int J Biol Macromol*. 2018;**109**:273–86. doi: 10.1016/j.ijbiomac.2017.12.078. [PubMed: 29248555].
33. Wang F, Li J, Tang X, Huang K, Chen L. Polyelectrolyte three layer nanoparticles of chitosan/dextran sulfate/chitosan for dual drug delivery. *Colloids Surf B Biointerfaces*. 2020;**190**:110925. doi: 10.1016/j.colsurfb.2020.110925. [PubMed: 32155455].
34. Sharif S, Abbas G, Hanif M, Bernkop-Schnurch A, Jalil A, Yaqoob M. Mucoadhesive micro-composites: Chitosan coated halloysite nanotubes for sustained drug delivery. *Colloids Surf B Biointerfaces*. 2019;**184**:110527. doi: 10.1016/j.colsurfb.2019.110527. [PubMed: 31577976].
35. Fookes FA, Mengatto LN, Rigalli A, Luna JA. Controlled fluoride release for osteoporosis treatment using orally administered chitosan hydrogels. *J Drug Deliv Sci Technol*. 2019;**51**:268–75. doi: 10.1016/j.jddst.2019.03.004.
36. Afshar M, Dini G, Vaezifar S, Mehdikhani M, Movahedi B. Preparation and characterization of sodium alginate/polyvinyl alcohol hydrogel containing drug-loaded chitosan nanoparticles as a drug delivery system. *J Drug Deliv Sci Technol*. 2020;**56**:101530. doi: 10.1016/j.jddst.2020.101530.
37. Zare-Akbari Z, Farhadnejad H, Furughi-Nia B, Abedin S, Yadollahi M, Khorsand-Ghayeni M. PH-sensitive bionanocomposite hydrogel beads based on carboxymethyl cellulose/ZnO nanoparticle as drug carrier. *Int J Biol Macromol*. 2016;**93**(Pt A):1317–27. doi: 10.1016/j.ijbiomac.2016.09.110. [PubMed: 27702657].
38. Hossieni-Aghdam SJ, Foroughi-Nia B, Zare-Akbari Z, Mojarad-Jabali S, Motasadizadeh H, Farhadnejad H. Facile fabrication and characterization of a novel oral pH-sensitive drug delivery system based on CMC hydrogel and HNT-AT nanohybrid. *Int J Biol Macromol*. 2018;**107**(Pt B):2436–49. doi: 10.1016/j.ijbiomac.2017.10.128. [PubMed: 29101044].
39. Schexnailder P, Schmidt G. Nanocomposite polymer hydrogels. *Colloid Polym Sci*. 2008;**287**(1):1–11. doi: 10.1007/s00396-008-1949-0.
40. Satarkar NS, Biswal D, Hilt J. Hydrogel nanocomposites: a review of applications as remote controlled biomaterials. *Soft Matter*. 2010;**6**(11):2364. doi: 10.1039/b925218p.
41. Hou D, Hu S, Huang Y, Gui R, Zhang L, Tao Q, et al. Preparation and in vitro study of lipid nanoparticles encapsulating drug loaded montmorillonite for ocular delivery. *Appl Clay Sci*. 2016;**119**:277–83. doi: 10.1016/j.clay.2015.10.028.
42. Tian H, Wang K, Liu D, Yan J, Xiang A, Rajulu AV. Enhanced mechanical and thermal properties of poly (vinyl alcohol)/corn starch blends by nanoclay intercalation. *Int J Biol Macromol*. 2017;**101**:314–20. doi: 10.1016/j.ijbiomac.2017.03.111. [PubMed: 28341175].
43. Wang R, Peng Y, Zhou M, Shou D. Smart montmorillonite-polypyrrole scaffolds for electro-responsive drug release. *Appl Clay Sci*. 2016;**134**:50–4. doi: 10.1016/j.clay.2016.05.004.
44. Yan H, Chen X, Bao C, Yi J, Lei M, Ke C, et al. Synthesis and assessment of CTAB and NPE modified organo-montmorillonite for the fabrication of organo-montmorillonite/alginate based hydrophobic pharmaceutical controlled-release formulation. *Colloids Surf B Biointerfaces*. 2020;**191**:110983. doi: 10.1016/j.colsurfb.2020.110983. [PubMed: 32208326].
45. Garcia-Guzman P, Medina-Torres L, Calderas F, Bernad-Bernad MJ, Gracia-Mora J, Mena B, et al. Characterization of hybrid microparticles/Montmorillonite composite with raspberry-like morphology for Atorvastatin controlled release. *Colloids Surf B Biointerfaces*. 2018;**167**:397–406. doi: 10.1016/j.colsurfb.2018.04.020. [PubMed: 29702471].
46. Kevadiya BD, Rajkumar S, Bajaj HC, Chettiar SS, Gosai K, Brahmbhatt H, et al. Biodegradable gelatin-ciprofloxacin-montmorillonite composite hydrogels for controlled drug release and wound dressing application. *Colloids Surf B Biointerfaces*. 2014;**122**:175–83. doi: 10.1016/j.colsurfb.2014.06.051. [PubMed: 25033437].
47. Lin FH, Lee YH, Jian CH, Wong JM, Shieh MJ, Wang CY. A study of purified montmorillonite intercalated with 5-fluorouracil as drug carrier. *Biomaterials*. 2002;**23**(9):1981–7. doi: 10.1016/s0142-9612(01)00325-8. [PubMed: 11996039].
48. Joshi GV, Kevadiya BD, Patel HA, Bajaj HC, Jasra RV. Montmorillonite as a drug delivery system: intercalation and in vitro release of timolol maleate. *Int J Pharm*. 2009;**374**(1-2):53–7. doi: 10.1016/j.ijpharm.2009.03.004. [PubMed: 19446759].
49. Iliescu RI, Andronescu E, Ghitulica CD, Voicu G, Ficai A, Hoteteu M. Montmorillonite-alginate nanocomposite as a drug delivery system–incorporation and in vitro release of irinotecan. *Int J Pharm*. 2014;**463**(2):184–92. doi: 10.1016/j.ijpharm.2013.08.043. [PubMed: 23998956].
50. Li J, Wang H, Yang B, Xu L, Zheng N, Chen H, et al. Control-release microcapsule of famotidine loaded biomimetic synthesized mesoporous silica nanoparticles: Controlled release effect and enhanced stomach adhesion in vitro. *Mater Sci Eng C Mater Biol Appl*. 2016;**58**:273–7. doi: 10.1016/j.msec.2015.08.031. [PubMed: 26478311].
51. Khalifa AM, Abdul Rasool BK. Optimized Mucoadhesive Coated Niosomes as a Sustained Oral Delivery System of Famotidine. *AAPS PharmSciTech*. 2017;**18**(8):3064–75. doi: 10.1208/s12249-017-0780-7. [PubMed: 28516414].
52. Singhavi DJ, Pundkar RS, Khan S. Famotidine microspheres reconstituted with floating in situ gel for stomach-specific delivery: Preparation and characterization. *J Drug Deliv Sci Technol*. 2017;**41**:251–9. doi: 10.1016/j.jddst.2017.07.017.
53. Alves JL, Rosa PDTVE, Morales AR. A comparative study of different routes for the modification of montmorillonite with ammonium and phosphonium salts. *Appl Clay Sci*. 2016;**132-133**:475–84. doi: 10.1016/j.clay.2016.07.018.
54. Fatahi Y, Sanjabi M, Rakhshani A, Motasadizadeh H, Darbasizadeh B, Bahadorikhalili S, et al. Levofloxacin-halloysite nanohybrid-loaded fibers based on poly (ethylene oxide) and sodium alginate: Fabrication, characterization, and antibacterial property. *J Drug Deliv Sci Technol*. 2021;**64**:102598. doi: 10.1016/j.jddst.2021.102598.
55. Ali S, Rajendran S, Joshi M. Synthesis and characterization of chitosan and silver loaded chitosan nanoparticles for bioactive polyester. *Carbohydr Polym*. 2011;**83**(2):438–46. doi: 10.1016/j.carbpol.2010.08.004.
56. Knaul JZ, Hudson SM, Creber KA. Improved mechanical properties of chitosan fibers. *J Appl Polym Sci*. 1999;**72**(13):1721–32. doi: 10.1002/(sici)1097-4628(19990624)72:13<1721::aid-app8>3.0.co;2-v.
57. Xu Y, Du Y. Effect of molecular structure of chitosan on protein delivery properties of chitosan nanoparticles. *Int J Pharm*. 2003;**250**(1):215–26. doi: 10.1016/s0378-5173(02)00548-3. [PubMed: 12480287].
58. Sureshkumar MK, Das D, Mallia MB, Gupta PC. Adsorption of uranium from aqueous solution using chitosan-

tripolyphosphate (CTPP) beads. *J Hazard Mater*. 2010;**184**(1-3):65–72. doi: 10.1016/j.jhazmat.2010.07.119. [PubMed: 20817347].
59. Borralleras P, Segura I, Aranda MA, Aguado A. Influence of experimental procedure on d-spacing measurement by XRD of montmorillonite clay pastes containing PCE-based superplasticizer. *Cem Concr Res*. 2019;**116**:266–72. doi: 10.1016/j.cemconres.2018.11.015.
60. Wu L, Lv G, Liu M, Wang D. Drug release material hosted by natural montmorillonite with proper modification. *Appl Clay Sci*. 2017;**148**:123–30. doi: 10.1016/j.clay.2017.07.034.
61. Jain S, Datta M. Oral extended release of dexamethasone: Montmorillonite–PLGA nanocomposites as a delivery vehicle. *Appl Clay Sci*. 2015;**104**:182–8. doi: 10.1016/j.clay.2014.11.028.
62. Perpétuo GL, Gálico DA, Fugita RA, Castro RAE, Eusébio MES, Treu-Filho O, et al. Thermal behavior of some antihistamines. *J Therm Anal Calorim*. 2012;**111**(3):2019–28. doi: 10.1007/s10973-012-2247-0.
63. Tao Y, Pan J, Yan S, Tang B, Zhu L. Tensile strength optimization and characterization of chitosan/TiO2 hybrid film. *Mater Sci Eng B*. 2007;**138**(1):84–9. doi: 10.1016/j.mseb.2006.12.013.
64. Berger J, Reist M, Mayer JM, Felt O, Peppas NA, Gurny R. Structure and interactions in covalently and ionically crosslinked chitosan hydrogels for biomedical applications. *Eur J Pharm Biopharm*. 2004;**57**(1):19–34. doi: 10.1016/s0939-6411(03)00161-9.